

# RSC Advances

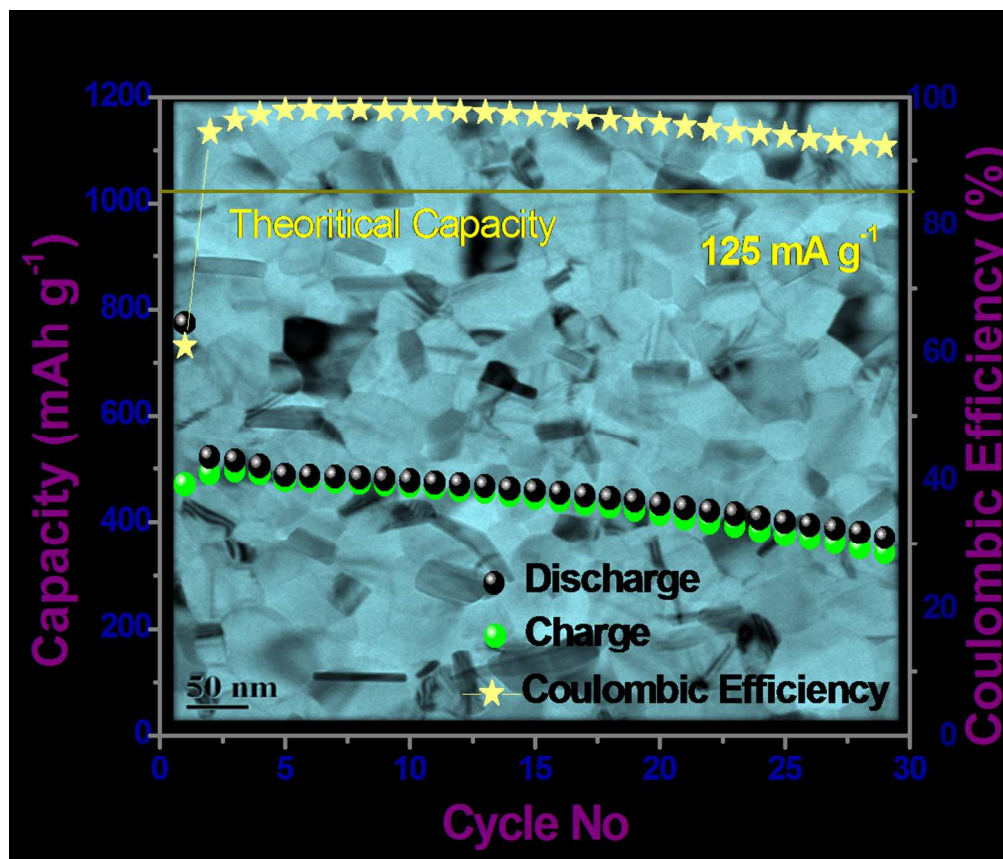


This is an *Accepted Manuscript*, which has been through the Royal Society of Chemistry peer review process and has been accepted for publication.

*Accepted Manuscripts* are published online shortly after acceptance, before technical editing, formatting and proof reading. Using this free service, authors can make their results available to the community, in citable form, before we publish the edited article. This *Accepted Manuscript* will be replaced by the edited, formatted and paginated article as soon as this is available.

You can find more information about *Accepted Manuscripts* in the [Information for Authors](#).

Please note that technical editing may introduce minor changes to the text and/or graphics, which may alter content. The journal's standard [Terms & Conditions](#) and the [Ethical guidelines](#) still apply. In no event shall the Royal Society of Chemistry be held responsible for any errors or omissions in this *Accepted Manuscript* or any consequences arising from the use of any information it contains.



SnS nanostructured anode for high performance sodium ion battery without any in-situ conductive coating and expensive additive stabilizer in electrolyte  
201x171mm (150 x 150 DPI)

## ARTICLE

# Excellent Electrochemical Performance of Tin Monosulphide (SnS) as Sodium-ion Battery Anode

Cite this: DOI: 10.1039/x0xx00000x

Prasit Kumar Dutta, Uttam Kumar Sen and Sagar Mitra\*

Received 00th January 2012,

Accepted 00th January 2012

DOI: 10.1039/x0xx00000x

[www.rsc.org/](http://www.rsc.org/)

Tin monosulphide was synthesized by a simple wet chemical synthesis approach. The as prepared tin mono sulphides used as anode in Na-ion batteries without any in situ conductive carbon or graphene coating and the electrode exhibited a high reversible sodium reversible capacity of  $\sim 500$  mAh  $g^{-1}$  at a discharge rate of 125 mA  $g^{-1}$ . It also demonstrated excellent high rate performance (*i.e.* 390 and 300 mAh  $g^{-1}$  at 500 and 1000 mA  $g^{-1}$  current density respectively) and cycle stability without addition of any expensive additive stabilizer like fluoroethylene carbonate (FEC) in compare to current literature.

## Introduction

It is certain that energy storage technology will be a determining technology to solve the present fuel and environmental crisis in future. Among all energy storage technologies, battery technology plays an important role in penetration of renewable sources to the electricity sector. The main player in battery technology, lithium battery is somewhat restricted due to high ore processing cost, fabrication cost and availability<sup>1</sup>. On the other hand, sodium or sodium-ion battery could be a great player in large scale sector due to nature abundant, low cost processing and suitable redox potential compare to Li ( $E^\circ$  value for  $Li/Li^+ = 3.05$  V and for  $Na/Na^+ = 2.71$  V vs. SHE at 298 K, 1 M, 1 atm). Recent trend shows that electrochemical cells based on sodium hold promises as large scale power sources because of their low cost and widespread geological distribution of sodium mines<sup>2</sup>. However, the practical implementation of sodium ion battery is somewhat limited due to its low energy density, poor cyclability, which is mainly attributed to large ionic radius of sodium ion<sup>3</sup>. In comparison to lithium ion, radius of sodium ion is 55% larger<sup>4</sup>, that makes it difficult to diffuse in most of the layered transition metal based oxide cathodes (sluggish sodium kinetics) and also causes large structural changes in the host electrodes<sup>5</sup>. This problem is more acute in case of anode, where intercalation of sodium ion in any form of graphite is almost impossible causing sodium electroplating on the surface rather than intercalation into basal planes of carbon electrode<sup>6</sup>.

In present scenario, utmost consideration for sodium-ion battery anode materials research is towards finding a sustainable, low-cost, non-toxic, non-explosive system to make a commercially viable sodium-ion battery. In current literature, many electrode materials such as hard carbon<sup>6</sup>, titanium oxide<sup>7</sup>, tin<sup>8, 9</sup>, antimony<sup>10</sup>, tin-tin sulphide-carbon composite<sup>9</sup>, tin disulphide-graphene composite<sup>11</sup>, red phosphorous-carbon composite<sup>12</sup>, and sodium terephthalate<sup>13</sup> were used and considered as a promising alternative anode to graphite and most of them suffer from rate capability and cyclic stability issues. In

recent studies, we have witnessed that alloy-based anode like Sn<sup>8, 9, 14</sup>, Sb<sup>10</sup>, Pb<sup>15</sup> and P<sup>12</sup> systems are most promising alternative, due to their high energy densities. However, these systems suffer from poor cyclic performance due to huge volume change occurred during alloying/dealloying reaction. Wang *et al.* have experimentally found that Sn can expand to 420% by volume after reacting with sodium and forming Na<sub>15</sub>Sn<sub>4</sub> phase causing electrode destabilization<sup>16</sup>. Apart from poor cyclic stability, the sluggish diffusion of Na-ion into solid medium at ambient temperature is a high barrier to overcome before its penetration to large scale applications.

In search of high capacity, high rate capable, safe and low cost anode materials, we have identified tin mono sulphide (SnS) as a conversion-cum-alloy based anode material for sodium ion batteries. Tin alone can store capacity of about 847 mAh  $g^{-1}$  (theoretical) due to formation of sodium rich Na<sub>15</sub>Sn<sub>4</sub> phase, whereas tin sulphide (SnS) phase can store capacity of about 1022 mAh  $g^{-1}$  (theoretical) with respect to Na. In current study, we have prepared tin mono sulphide nanoparticles with occasional nanorods using a simple wet chemical synthesis route at room temperature, followed by annealing with SnCl<sub>2</sub> as tin source and thioacetamide as sulphur source respectively. The bare SnS material was used as electro-active material without any conductive coating and tested in half-cell configuration against Na using 1 M NaClO<sub>4</sub> in propylene carbonate (without any additive stabilizer) as electrolyte. In current study, sodium alginate is used as an interactive binder<sup>17, 18</sup> to buffer such high volume expansion during alloying-dealloying reactions and observed high stability in electrode performance. The electrode material is able to exhibit 325 mAh  $g^{-1}$  reversible capacity even after thirty cycles at 125 mA  $g^{-1}$  current rate. To our best knowledge, first time we are reporting synthesized bare SnS as sodium-ion battery anode with excellent rate capability compare to existing literature.

## Experimental Section

## Synthesis of SnS

A simple wet chemical synthesis process was adopted<sup>19</sup> to prepare SnS nano-rods. In a typical synthesis process, ~ 3.0 mM of SnCl<sub>2</sub>·2H<sub>2</sub>O (99%, Merck, India) was dissolved in 5 ml of acetone (99%, Merck, India). Then 7.5 ml of triethanolamine solution was added in equal amount of deionised water and the diluted triethanolamine solution was added to SnCl<sub>2</sub> solution under constant stirring. Finally, 5 ml 1M thioacetamide (99%, Spectrochem, India) solution was added followed by the addition of 25 ml 4M ammonia solution (28%, Merck, India). The reaction mixture was allowed to stir around 16 hours in closed beaker at room temperature. Dark brown precipitate was obtained which was further centrifuged, washed for several times with deionised water, dried at 60°C in hot air oven for 12 hours and finally annealed at 500°C for 5 hours under N<sub>2</sub> atmosphere.

## Material Characterisation

Material characterisation was done by powder X-ray diffraction (XRD) measurements at 25 °C using Philips X'-pert Diffractometer, with Cu K $\alpha$  radiation ( $\lambda = 1.5418 \text{ \AA}$ ) at 40 kV and 40 mA. Morphological analysis was carried out using JEOL-2100F field emission gun transmission electron microscope (FEG-TEM). For TEM analysis, a well-dispersed solution was prepared by adding a little amount of SnS powder in isopropyl alcohol and sonicated for 30 min. One drop of dispersed solution was taken on TEM grid to obtain high resolution images at the best operating condition. Energy dispersive X-ray analysis (EDAX) was performed to estimate the atomic proportion of the as synthesized material.

## Electrochemical Cell Fabrication and Measurements

Galvanostatic charge-discharge tests were carried out using lab scale Swagelok type cells having a cell configuration of Na|NaClO<sub>4</sub>|SnS. Electrochemical cells were assembled in an argon-filled glovebox (Lab Star, Mbraun, Germany) with controlled moisture and oxygen concentration around 1 ppm. Sodium foil was used as a counter as well as reference electrode. For electrolyte preparation, sodium perchlorate (NaClO<sub>4</sub>) salt was dissolved in propylene carbonate (PC) to obtain a 1M NaClO<sub>4</sub> solution which was used as an electrolyte in this study. The electrolyte preparation was done inside the argon filled glovebox. Borosilicate glass microfiber filters (Whatman) were used as a separator. The electrodes were prepared using SnS as the active material, carbon black (Super C-65, Timal, Switzerland) as conductive additive, and a polymeric binder (sodium alginate) with an overall ratio of 3:1:1 (by wt.). Slurry was prepared by adding hand-grinded mixture of SnS and carbon in sodium alginate jellified with few drops of deionized water, under a constant stirring for 4 h at room temperature. This slurry was then cast on Cu foil using doctor's blade and the electrode was dried at 60 °C under vacuum for 12 h. Cyclic voltammetry (CV) profile was obtained by measuring *i*-*V* response at scan rate of 0.1 mV s<sup>-1</sup> within potential window of 0.1-2.0 V vs. Na/Na<sup>+</sup>, using Biologic VMP-3 potentiostat/galvanostat. The electrochemical charge-discharge experiments were performed using Arbin Instrument, USA (BT2000 model) at various constant current rates. Potentiostatic electrochemical impedance spectroscopy (PEIS) was done for the first discharge and charge cycle at ten different points within a frequency range of 1 MHz to 0.1 Hz and with voltage amplitude of  $\Delta V = 5 \text{ mV}$  using Biologic VMP-3 instrument. For EIS experiments, charge-discharge was carried out at a constant current density of 50 mA g<sup>-1</sup>. All

the electrochemical measurements were done at a constant temperature of 20 °C.

## Results and Discussion

### Structural Characterization

X-ray diffraction (XRD) pattern of SnS powder is shown in Fig. 1a, which is indexed as orthorhombic phase of SnS (JCPDS card No. 75-2115). It is noteworthy to specify that the as obtained SnS is not 100% phase pure but contain some impurities of SnS<sub>x</sub><sup>20</sup>. High-resolution transmission electron microscopy instrument was used to study the microstructure of SnS sample. FEG-TEM images (shown in Fig. 1b,d-g) illustrates that nanoparticle with occasional nanorod type morphology of SnS was obtained with particle size <100 nm. The high resolution images (Fig. 1d and 1e) identify that the well-defined layered structure of SnS, having an interlayer distance of 0.312 nm for (210) planes and 0.252 nm for (211) planes have been observed. Selected area electron diffraction (SAED) pattern shown in Fig. 1c indicates the planes corresponding to (0 1 1), (1 1 1), (4 1 1) planes of orthorhombic SnS crystal. EDAX analysis (Fig. S1 in supporting information) shows that 1:1 atomic ratio of Sn and S are present in the as prepared SnS sample.

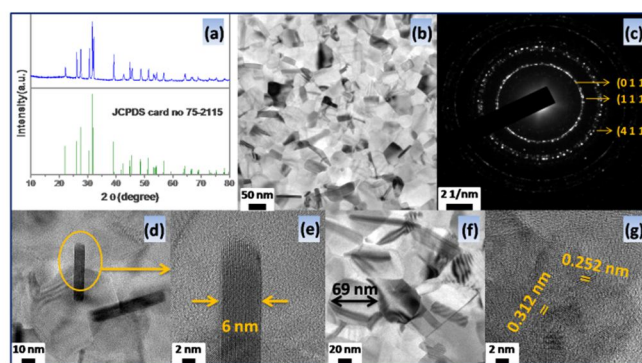


Fig. 1: (a) XRD pattern, (b, d-g) FEG-TEM images, (c) selected area electron diffraction (SAED) pattern (corresponding to Fig. 1b) of as synthesized SnS.

### Electrochemical performance

The reaction of SnS with sodium is bit complicated as it undergoes conversion first and then alloying reaction with sodium. In this system both Sn and S undergo alloying reaction with sodium. Therefore, a careful investigation was carried out to understand the sodium storage mechanism in SnS. Fig. 2a shows the cyclic voltammogram of SnS electrode performed in a voltage window of 0.1–2 V vs. Na/Na<sup>+</sup> at voltage scan of 0.02 mV s<sup>-1</sup>. During the first cathodic sweep, two prominent peaks were observed at 0.75 V and 0.2 V vs. Na/Na<sup>+</sup>, respectively. As per literature, the peak at 0.75 V is associated with both conversion reaction (SnS to Sn and Na<sub>2</sub>S) as well as alloying reaction (with Sn<sup>3+,8</sup>). As both the conversion reaction of SnS and alloying reaction of Sn are occurred at ~ 0.7 V vs. Na/Na<sup>+</sup>, so it is difficult to distinguish the conversion and alloying peaks. Furthermore, the peak at 0.2 V was due to the reaction between Na and NaSn alloy. The alloying reaction between Na and Sn is known to be multistep reaction<sup>16</sup>. In the first step (at ~ 0.7 V), Sn forms alloy with Na and form Na<sub>9</sub>Sn<sub>4</sub><sup>3,16</sup>. During anodic sweep three prominent peaks were observed at 0.2V, 0.65 V and 1.0V

vs.  $\text{Na}/\text{Na}^+$  along with two small humps at 1.3 V and 1.7 V vs.  $\text{Na}/\text{Na}^+$  respectively. The peaks at 0.2 V and 0.65 V were due to the two step dealloying reaction from  $\text{NaSn}_x$ , whereas; the peak at 1.0 V was due to the formation of  $\text{SnS}_x$ <sup>21</sup>. The small humps at 1.3 V and 1.7 V were due to formation of polysulphur form  $\text{Na}_2\text{S}_x$ <sup>22</sup>.

It was found that after 1<sup>st</sup> cycle free sulphur and metal nanoparticles were present in the system which were utilized to ensnare sodium. Similar kind of mechanism was also observed in other metal sulphide based anodes<sup>21, 23-25</sup>. The so obtained CV profile showing Fig. 2a demonstrates the change in the voltammogram from 1<sup>st</sup> cycle to the remaining cycles. During the second cathodic sweep three prominent redox peaks were observed at 1.1 V, 0.7 V and at 0.2 V vs.  $\text{Na}/\text{Na}^+$  respectively. The peak at 1.1 V is due to the reaction Na and polysulphur to form  $\text{Na}_2\text{S}_x$  whereas the peaks at 0.7 V and 0.2 V were due to the alloying reaction between sodium and tin. During the reverse process (2<sup>nd</sup> anodic sweep), four peaks were observed at 0.2 V, 0.65 V, 1.3 V and 1.7 V vs.  $\text{Na}/\text{Na}^+$  respectively. The intense peak at 0.2 V and 0.65 V were due to the dealloying reaction of  $\text{NaSn}_x$  reaction. The peak at 1.3 V and 1.7 V were due to formation polysulphur. Similar observations were noticed during the charge-discharge cycling shown in Fig. 2b.

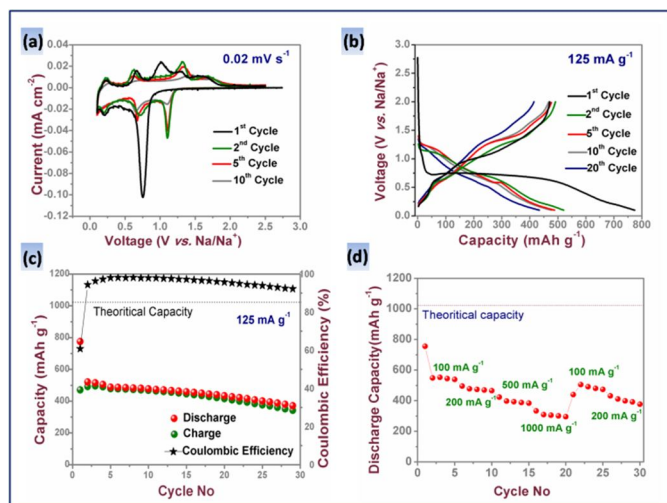


Fig. 2: (a) Cyclic voltammetry at a scan rate of  $0.02 \text{ mV s}^{-1}$ , (b) charge-discharge profile at current rate of  $125 \text{ mA g}^{-1}$ , (c) cyclic performance at  $125 \text{ mA g}^{-1}$  and (d) power cycle performance of  $\text{Na}|\text{NaClO}_4|\text{SnS}$  half-cell within the potential range of 0.1 to 2 V.

### Rate performance test

Fig. 2b-d shows galvanostatic charge-discharge profiles that was carried out at constant as well as variable current densities within the potential range of 2.0 to 0.1 V vs.  $\text{Na}/\text{Na}^+$ . Initial discharge capacity of  $\sim 775 \text{ mAh g}^{-1}$  was obtained at a discharge rate of  $125 \text{ mA g}^{-1}$  ( $\sim \text{C}/8$  rate), while a reversible capacity of  $\sim 500 \text{ mAh g}^{-1}$  was achieved after few charge-discharge cycles. At the end of 30 cycles, a discharge capacity  $\sim 370 \text{ mAh g}^{-1}$  retained which is about 74% of the reversible capacity of 1<sup>st</sup> cycle. A high coulombic efficiency of around 98% was estimated for the initial 15 cycles which indicates a better performance of the electrode. After 15 cycles, a gradual declining nature in discharge capacity as well as the coulombic efficiency was obtained which mainly due to material loss caused by volume expansion related issues such as cracking and pulverization of the electrode. Power cycle performance shown in Fig. 2c describe that at high rate of  $500 \text{ mA g}^{-1}$  and  $1000 \text{ mA g}^{-1}$  a reversible capacity of 390 and 300

$\text{mAh g}^{-1}$  have been achieved with bare electrode material. As per best of our knowledge there are no matching results available in the literature that show bare SnS was used as anode for Sodium-ion batteries to compare the rate capability. A comparison of electrochemical performance between electrodes with different composition of 60:20:20 and 70:20:10 was performed and shown in Fig. S2 as supporting information. The morphology of the electrode after charge-discharge cycle was also investigated (Fig. S3 & S4 in supporting information), which shows that the initial morphology was changed after 30 cycles.

Further understanding the interfacial properties, electrochemical impedance spectroscopy (EIS) experiment was carried out (Fig. 3a and b) to realize the change in the electrode reaction. During the first discharge-charge process EIS was taken at five different points (Fig. 3c) in each half cycle. It was observed that charge transfer resistance of the electrode was increased from OCV to 0.8 V which may be due to Na insertion in the SnS lattice. Electrode impedance was even increased upon moving to the conversion region and then mostly stable thereafter. During the oxidation process (charge reaction) three process were observe, first dealloying of Na from  $\text{Na}_x\text{Sn}$  followed by formation of  $\text{SnS}_x$  and finally formation of polysulphur from  $\text{Na}_2\text{S}$ . Dealloying reaction was occurred in two steps at  $\sim 0.3$  and  $\sim 0.7$  V. So when EIS was taken at 0.5V two semicircles were observed due to presence of two phasic components. At the end the dealloying reaction (at 0.8V) EIS shows that the second semicircle was disappeared. After 0.8 V  $\text{SnS}_x$  was formed from Sn and  $\text{Na}_2\text{S}$  which was evident by the change in the charge transfer resistance. An increasing trend in the charge transfer resistance value was found at 1.2 V due to removal of metallic nanoparticles from the system. Finally a two-step polysulphur formation reaction was took place at  $\sim 1.4$  V and  $\sim 1.6$  V. Therefore, at 1.5 V the possibility of presence of two phasic components was indicated by the evolution of an extra semicircle which was disappeared after completion of the reaction (at 2.0 V).

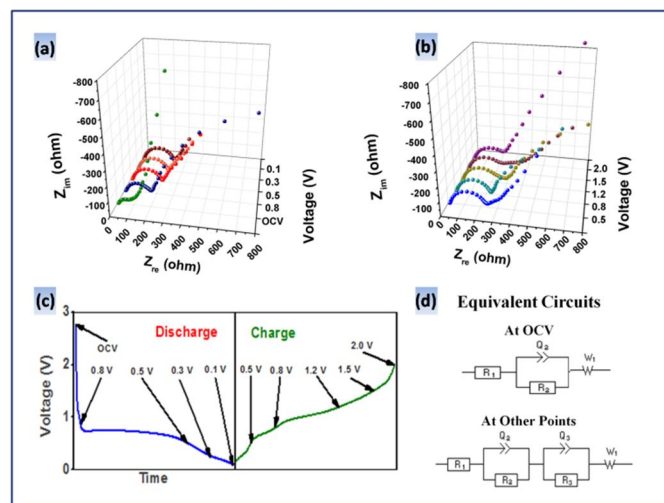


Fig. 3: EIS spectra of SnS electrode at different potential during (a) 1<sup>st</sup> discharge and (b) charge process, (c) charge-discharge profile of 1<sup>st</sup> cycle at  $50 \text{ mA g}^{-1}$  along with potential points where EIS were taken, (d) the equivalent circuit used to fit the EIS spectra.

### Conclusions

In summary, we have successfully synthesized nanostructured SnS electrode via simple solution based technique. In current

study, we have not applied any conducting coating to the sample to improve the electrode kinetics further and used directly as anode material for sodium ion battery. A stable electrochemical performance was achieved using 1M NaClO<sub>4</sub> in PC without any additive. High reversible capacity due to conversion and alloying reaction of the SnS based electrode was demonstrated using constant current charge-discharge and power cycling. The bare SnS electrode showed excellent rate performance with reversible capacity of ~ 370-520 mAh g<sup>-1</sup> at a discharge rate of 125 mA g<sup>-1</sup>. The good electrochemical performance is attributed to the unique morphology with larger interlayer distance, and easy fuelling of electrons at the electrode-electrolyte interface. Electrochemical impedance spectroscopy and slow scan cyclic voltammetry experiments were used to insight the complicated reaction mechanism with sodium. Both the experiment has come to a same conclusion and elucidates the mechanism. Furthermore, we have used sodium-alginate binder to stabilize the cycle. The increase in rate performance may further improve by use of optimized electrolyte and altering the electrode fabrication technology.

### Acknowledgements

The authors acknowledge the financial support provided by Solar Energy Research Institute for India and the United (SERIUS) funded by the U.S. Department of Energy (Office of Science, Office of Basic Energy Sciences, and Energy Efficiency and Renewable Energy, Solar Energy Technology Program, under Subcontract DEAC36-08GO28308 to the National Renewable Energy Laboratory.

### Notes and references

Electrochemical Energy Laboratory, Department of Energy Science and Engineering, Indian Institute of Technology Bombay, Powai, Mumbai 400076, India.

\* E-mail: [sagar.mitra@iitb.ac.in](mailto:sagar.mitra@iitb.ac.in);

Fax: +91-22-2576-4890; Tel: +91-22-2576-7849

† Electronic Supplementary Information (ESI) available: [details of any supplementary information available should be included here]. See DOI: 10.1039/b000000x/

1. B. Scrosati, *Nature*, 2011, **473**, 448.
2. G. D. Aumann and J. T. Emlen, *Nature*, 1965, **208**, 198.
3. V. L. Chevrier and G. Ceder, *J. Electrochem. Soc.*, 2011, **158**, A1011.
4. L. Xiao, Y. Cao, J. Xiao, W. Wang, L. Kovarik, Z. Nie and J. Liu, *Chem. Commun.*, 2012, **48**, 3321.
5. S.-W. Kim, D.-H. Seo, X. Ma, G. Ceder and K. Kang, *Adv. Energy Mater.*, 2012, **2**, 710.
6. D. A. Stevens and J. R. Dahn, *J. Electrochem. Soc.*, 2000, **147**, 1271.
7. H. Xiong, M. D. Slater, M. Balasubramanian, C. S. Johnson and T. Rajh, *J. Phys. Chem. Lett.*, 2011, **2**, 2560.
8. Y.-M. Lin, P. R. Abel, A. Gupta, J. B. Goodenough, A. Heller and C. B. Mullins, *ACS Appl. Mater. Interfaces*, 2013, **5**, 8273.
9. L. Wu, X. Hu, J. Qian, F. Pei, F. Wu, R. Mao, X. Ai, H. Yang and Y. Cao, *J. Mater. Chem. A*, 2013, **1**, 7181.
10. J. Qian, Y. Chen, L. Wu, Y. Cao, X. Ai and H. Yang, *Chem. Commun.*, 2012, **48**, 7070.

11. X. Xie, D. Su, S. Chen, J. Zhang, S. Dou and G. Wang, *Chem.–Asian J.*, 2014, **9**, 1611.
12. Y. Kim, Y. Park, A. Choi, N.-S. Choi, J. Kim, J. Lee, J. H. Ryu, S. M. Oh and K. T. Lee, *Adv. Mater.*, 2013, **25**, 3045.
13. L. Zhao, J. Zhao, Y.-S. Hu, H. Li, Z. Zhou, M. Armand and L. Chen, *Adv. Energy Mater.*, 2012, **2**, 962.
14. S. Komaba, Y. Matsuura, T. Ishikawa, N. Yabuuchi, W. Murata and S. Kuze, *Electrochem. Commun.*, 2012, **21**, 65.
15. M. Mortazavi, J. Deng, V. B. Shenoy and N. V. Medhekar, *J. Power Sources*, 2013, **225**, 207.
16. J. W. Wang, X. H. Liu, S. X. Mao and J. Y. Huang, *Nano Lett.*, 2012, **12**, 5897.
17. P. S. Veluri and S. Mitra, *RSC Adv.*, 2013, **3**, 15132.
18. I. Kovalenko, B. Zdyrko, A. Magasinski, B. Hertzberg, Z. Milicev, R. Burtovyy, I. Luzinov and G. Yushin, *Science*, 2011, **334**, 75.
19. A. J. Ragina, K. V. Murali, K. C. Preetha, K. Deepa and T. L. Remadevi, *J. Mater. Sci: Mater. El.*, 2012, **23**, 2264.
20. A. M. Tripathi and S. Mitra, *RSC Adv.*, 2014, **4**, 10358.
21. B. Qu, C. Ma, G. Ji, C. Xu, J. Xu, Y. S. Meng, T. Wang and J. Y. Lee, *Adv. Mater.*, 2014, **26**, 3854.
22. J. Park, J.-S. Kim, J.-W. Park, T.-H. Nam, K.-W. Kim, J.-H. Ahn, G. Wang and H.-J. Ahn, *Electrochim. Acta*, 2013, **92**, 427.
23. D. Su, S. Dou and G. Wang, *Chem. Commun.*, 2014, **50**, 4192.
24. X. Fang, X. Guo, Y. Mao, C. Hua, L. Shen, Y. Hu, Z. Wang, F. Wu and L. Chen, *Chem.–Asian J.*, 2012, **7**, 1013.
25. X. Fang, C. Hua, X. Guo, Y. Hu, Z. Wang, X. Gao, F. Wu, J. Wang and L. Chen, *Electrochim. Acta*, 2012, **81**, 155.